AD-A172 230 EMISSIVITY AS A FUNCTION OF SURFACE ROUGHNESS: A COMPUTER MODEL(U) NAVAL RESEARCH LAB WASHINGTON DC I B SCHWARTZ ET AL. 29 AUG 86 NRL-MR-5816 1/1

UNCLASSIFIED F/G 20/6 NL

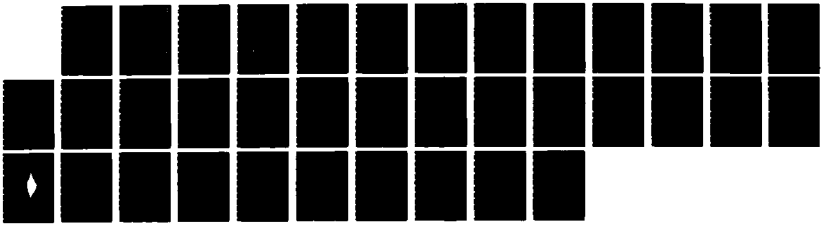

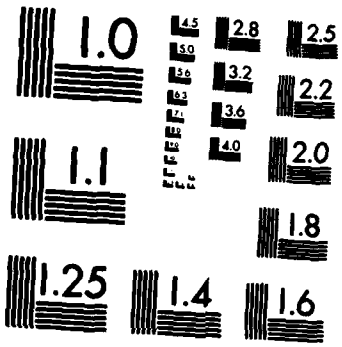

MICROCOPY RESOLUTION TEST CHART
NATIONAL BUREAU OF STANDARDS-1963-A

AD-A172 230

Emissivity as a Function of Surface Roughness: A Computer Model

IRA B. SCHWARTZ AND DAVID HON*

Advanced Concepts Branch
Optical Sciences Division

**Sachs/Freeman Assoc., Inc.*
Landover, MD 20785

DTIC
ELECTE
SEP 2 3 1986
S D
B

DTIC FILE COPY

Approved for public release; distribution unlimited.

86 9 23 091

SECURITY CLASSIFICATION OF THIS PAGE

AD-A172 230

REPORT DOCUMENTATION PAGE

1a. REPORT SECURITY CLASSIFICATION UNCLASSIFIED	1b. RESTRICTIVE MARKINGS
2a. SECURITY CLASSIFICATION AUTHORITY	3. DISTRIBUTION / AVAILABILITY OF REPORT Approved for public release; distribution unlimited.
2b. DECLASSIFICATION / DOWNGRADING SCHEDULE	
4. PERFORMING ORGANIZATION REPORT NUMBER(S) NRL Memorandum Report 5816	5. MONITORING ORGANIZATION REPORT NUMBER(S)
6a. NAME OF PERFORMING ORGANIZATION Naval Research Laboratory — 6b. OFFICE SYMBOL (If applicable) 6520	7a. NAME OF MONITORING ORGANIZATION
6c. ADDRESS (City, State, and ZIP Code) Washington, DC 20375-5000	7b. ADDRESS (City, State, and ZIP Code)
8a. NAME OF FUNDING / SPONSORING ORGANIZATION Office of Naval Research — 8b. OFFICE SYMBOL (If applicable)	9. PROCUREMENT INSTRUMENT IDENTIFICATION NUMBER
8c. ADDRESS (City, State, and ZIP Code) Arlington, VA 22217	10. SOURCE OF FUNDING NUMBERS PROGRAM ELEMENT NO. 61153N; PROJECT NO.; TASK NO.; WORK UNIT ACCESSION NO. DN380-425

11. TITLE (Include Security Classification)
Emissivity as a Function of Surface Roughness: A Computer Model

12. PERSONAL AUTHOR(S)
Ira B. Schwartz and David Hon*

13a. TYPE OF REPORT	13b. TIME COVERED	14. DATE OF REPORT (Year, Month, Day)	15. PAGE COUNT
Interim	FROM 9/84 TO 8/85	1986 August 29	36

16. SUPPLEMENTARY NOTATION
*Sachs/Freeman Assoc., Inc. Landover, MD 20785

17. COSATI CODES			18. SUBJECT TERMS (Continue on reverse if necessary and identify by block number)
FIELD	GROUP	SUB-GROUP	Emissivity, Surface roughness, Infrared, Sea surface modelling

19. ABSTRACT (Continue on reverse if necessary and identify by block number)

Surface geometry plays an important role in modelling backgrounds in the infrared. In particular, surface roughness of the ocean varies as a function of wind speed, and therefore it is important to realize the impact of surface roughness on self-emissions over a wide range of wavelengths and wind speeds. ~~In~~ this paper, ~~we~~ describe the results of a computer model used to generate a synthetic surface as a function of wind speed on the average emissivity of the given surface. Surfaces generated with varying spectral content are compared. Capillary waves are shown to have a measurable effect on the average emissivity of the ocean surface, and therefore should not be ignored when constructing a model of the ocean surface. Keywords:

20. DISTRIBUTION / AVAILABILITY OF ABSTRACT ☒ UNCLASSIFIED/UNLIMITED ☐ SAME AS RPT. ☐ DTIC USERS	21. ABSTRACT SECURITY CLASSIFICATION UNCLASSIFIED
22a. NAME OF RESPONSIBLE INDIVIDUAL Ira B. Schwartz	22b. TELEPHONE (Include Area Code) (202) 767-3799 — 22c. OFFICE SYMBOL Code 6522

DD FORM 1473, 84 MAR — 83 APR edition may be used until exhausted. All other editions are obsolete. — SECURITY CLASSIFICATION OF THIS PAGE

CONTENTS

0. INTRODUCTION 1

1. THE SEA SURFACE MODEL 3

2. EMISSIVITY AND TEMPERATURE COMPUTATIONS 7

3. GENERAL DISCUSSION 14

4. DISCUSSION OF PLOTS 16

5. CONCLUSIONS 18

6. REFERENCES 21

DTIC
ELECTE
SEP 2 3 1986
S D
B

Accession For
NTIS GRA&I
DTIC TAB
Unannounced
Justification
By
Distribution/
Availability Codes
Avail and/or
Dist Special
A-1

QUALITY INSPECTED 4

EMISSIVITY AS A FUNCTION OF SURFACE ROUGHNESS: A COMPUTER MODEL

0. INTRODUCTION : Recently, remote sensing of the earth and target recognition in a cluttered background have been making use of sophisticated modelling of the earth's oceans. Of particular importance in many applications of military and oceanographic nature is the determination of the sea surface temperature. For example, to make background clutter predictions, a spatial correlation of the temperature is required, and since the emissivity of water is angularly dependent , one needs to know the geometry of the surface at a given instant of time [7]. Since most probes directly measure the temperature well below the surface at only one point in space , most surface measurements are made radiometrically; i.e., a measure of radiance (intensity) is made, and if the emissivity and wavelength are known, a temperature can be computed from a blackbody formula [3,4,6,10,12,13] . Radiometric measurements can be done using satellites ,and therefore , large scale surface temperatures of the ocean can be made provided enough information about the environment is known as well as emissivity with respect to the surface. In this paper, we analyze the effect of sea surface roughness upon the emissivity of the surface. Particular attention will be paid to the short wavelength contributions assumed to be beyond the resolution of most infrared sensors.

Manuscript approved May 15, 1986.

The infrared radiance of the sea is described by two components: self emission and sky reflectance. Self emission for monochromatic radiation can be described by a gray body approximation [5,page 40]. As mentioned above, radiance measurements are used to infer surface temperature. For example, Singh and Warren [11] describe recent experiments in which sea-surface temperature is measured on a global scale using the Advanced Very High Resolution Radiometer from space. Sidran [10] also considers the influence of sea surface temperature from radiometry measurements. Assuming sky reflectance has been properly subtracted from the signal, we can derive an expression from the gray body formula and compute an indirectly measured temperature. For monochromatic radiation this measured temperature,T, of a small element of surface area is a function of emissivity and measured radiance . We investigate this relationship by assuming the entire surface is emitting at some fixed temperature and the emissivity is purely a function of surface roughness. Specifically, for a given flat horizontal element of surface, water has an emissivity that is a function of view angle with respect to the surface normal. Therefore, if we assume that the surface is composed of contiguous flat elements, the radiance of the surface depends upon the slope and orientation of each element of fluid surface. Under these assumptions, we demonstrate how the measured temperature of the surface depends upon its roughness. The procedure requires the following :

1.The development of an accurate sea surface model,where the model incorporates wind velocity as a parameter.

2.Computation of the surface emissivity from the model.

3.Subsequent inference of surface temperature.

The sea surface modelling follows the method outlined in [1a,14] with enhancements which allow for broader spectral resolution and surface self shadowing. Resulting computer calculations of emissivity are deterministic, compare favorably with the results of [10], and allow for high resolution image synthesis. Final inherent temperature dependance on surface roughness sheds some light on ship wake measurements [8] , and corrects some of the analysis of spatial sea surface temperature variation recently reported in [6] . The wind wave spectral dependance of surface emissivity also indicates that shorter wavelengths, such as capillary and Leyken/Rosenberg, generally not considered to be resolvable by infrared sensors, as assumed in [14], do indeed affect measurements.

1. The Sea Surface Model : As mentioned above, the method used to generate sea surfaces follows closely to what is outlined in [1a,14] . The first step is to define the power spectrum of a purely wind driven wave system. The

spectrum used is supplied by the Pierson-Stacy model [9]. We assume that the surface elevation can be expressed as the inverse Fourier transform (IFT) of the elevation;i.e.,

$$1\text{-}1 \qquad z = \iint_{-\infty}^{+\infty} c(\underset{\sim}{k}) \exp(2\pi i \underset{\sim}{k} \cdot \underset{\sim}{x}) d\underset{\sim}{k} \equiv \zeta(\underset{\sim}{x}) \ ,$$

where x and k are members of R^2, and c(k) is the Fourier transform of the elevation. The power spectral density and the amplitude of the Fourier transform are related by :

$$1\text{-}2 \qquad S(\underset{\sim}{k}) \propto |c(\underset{\sim}{k})|^2$$

where S(k) is the elevation (power) spectrum.

The spectrum contains most of the available information about the system. However, by definition, a power spectrum contains no phase dependance. Therefore, in order to create a reasonable model of the surface elevation, we assume that the phase relationship between Fourier components is uniformly random and write the Fourier transform function as:

$$1\text{-}3 \qquad c(\underset{\sim}{k}) \propto \sqrt{S(\underset{\sim}{k})}\, e^{i\phi(\underset{\sim}{k})} \ ,$$

where ϕ is a real random variable taking values between $-\pi$ and $+\pi$ and having a uniform probability density distribution. We require that the sea surface elevation function be a real valued function of x. Since our numerical inverse fast Fourier transform (IFFT) is a complex to

complex transformation, we construct the arbitrary phase components in such a fashion that the output of the two dimensional IFFT has imaginary components which are identically zero. This leads to the expressions for elevation and normal components of the surface:

$$\text{1-4a} \quad \zeta(\underset{\sim}{x}) \propto \iint_{-\infty}^{+\infty} [S(\underset{\sim}{k})]^{1/2} \exp(2\pi i \underset{\sim}{k}\cdot\underset{\sim}{x}) e^{i\phi(\underset{\sim}{k})} d\underset{\sim}{k}$$

$$\text{1-4b} \quad \text{grad}\zeta(\underset{\sim}{x}) \propto \iint_{-\infty}^{+\infty} i\underset{\sim}{k}[S(\underset{\sim}{k})]^{1/2} \exp(2\pi i \underset{\sim}{k}\cdot\underset{\sim}{x}) e^{i\phi(\underset{\sim}{k})} d\underset{\sim}{k} \quad .$$

$\phi(k)$ is the random variable described above and satisfies the anti-symmetry constraints:

$$\text{1-5a} \quad \phi(\underset{\sim}{k}) = \phi(k_1, k_2) = -\phi(-k_1, -k_2) \quad , \; 0 \le k_i \le k_{max} \quad , i=1,2$$

$$\text{1-5b} \quad \phi(-k_1, k_2) = -\phi(k_1, -k_2), \quad 0 \le k_i \le k_{max} \quad ,$$

$$\text{1-5c} \quad \phi(\underset{\sim}{k}) \equiv 0, \; k_1, k_2 > k_{max} \quad .$$

To calculate the two dimensional IFT we use the IMSL FFT routine fft3d on a vax11/780. This requires the matrix representation of the spectrum in cartesian coordinates (the

Pierson-Stacy spectrum is provided in polar form), with a careful selection of wave number range and array dimensions. According to Pierson and Stacy [9, Fig. 9.1 page 89), an integration of the slope spectrum over the wave number range 0.003 to 1.2 (1/cm) yields slope statistics which agree well with the Cox & Munk observations [2]. In order to approximate this range, and retain compatability with the FFT routine, a 512x512 array was used to define the spectrum.

The IFFT was applied to a normalized spectrum, for which the proportionality constant was set to unity. The normalization was then rescaled after application of the IFFT by requiring that the variance of the output array be equal to the elevation variance calculated directly from the spectrum.

The sea state surface is parameterized by wind velocity, and a maximum value of k, k_{max}, chosen for the FFT. There is a one-to-one correspondence between wind speed and elevation variance, hence the surface roughness of our sea-state is directly related to the wind speed.

Sea state surfaces for three spectral windows were constructed. A 'base-line' window, which we call the 'Cox-Munk' spectral window (see Fig. 1), has a power spectrum yielding slope statistics which are in good agreement with those of Cox & Munk. A second spectral window excludes the smaller wavelengths (less than 18 cm) of wind waves, which contribute little to the total energy of the spectrum (i.e.

total elevation variance), but contain the largest slope variance. This spectral window is called the sub-Leyken/Rosenberg spectral range. Finally,the third spectral window includes the entire range of capillary waves (note that the Cox-Munk spectral region only partly includes the capillary range. (In [9], Pierson & Stacy conclude that the Cox and Munk photographic measurements acted as a band pass filter). Precise wave numbers for the three spectral regions are shown in Table 1. For each spectral window, we constructed surface models (elevation and slope arrays) for the four wind speeds (3.46, 5.61, 7.63, 9.97 (m/s)) at elevation 19.5 m. A simple grid plot of the 9.97 m/s wind wave surface is shown in Fig. 2.

2. Emissivity & Temperature Computations :

For a smooth horizontal surface, the emissivity, ε, is described as follows. Let θ denote the angle between the viewing vector from the surface to the point of view and the surface normal. Then for $\theta \in [0,\pi/2]$ assume:

i. $\varepsilon(0) = 1$, and $\varepsilon(\theta) \to 0$ as $\theta \to \pi/2$.

ii. $\varepsilon'(\theta)<0$ and $\varepsilon''(\theta)>0$ for $\theta \in (0,\pi/2)$.

The emissivity water for a flat horizontal surface as a function of θ is shown in Fig. 3, and satisfies i and ii.

Given a general surface ,S, we parameterize a vector $X(t)$ on the surface , where $t = (t_1,t_2)$, and assume $X(0) = 0$. (see Fig. 4.) Let $r(X)$ denote a vector from X on S to the

point of view. (Note that $r(0)$ is a vector from the origin to the point of view.) The unit normal on S at X is given by

$$n(X(t)) = \frac{D_1 X(t) \times D_2 X(t)}{||D_1 X(t) \times D_2 X(t)||} .$$

For a given $r(0)$, let

$$\hat{\theta}(r(0)) = \arccos(r(0)\cdot e_3 / ||r(0)||) .$$

Thus the emissivity will be a function of the position of view to $X(0)$. Specifically, the emissivity over the surface will be a function of $\hat{\theta}$ at $r(0)$. Define $\theta(X(t))$ to be the $\arccos(n(X)\cdot r(X)/||r(X)||)$. The **MEAN EMISSIVITY for r(0) on S** is defined by the weighted average

$$\langle \hat{\varepsilon}(\theta(r(0))) \rangle = \frac{\int\int_S \varepsilon(\theta(X))\, \underset{\sim}{r}(X)\cdot \underset{\sim}{n}(X)\, \Psi(\underset{\sim}{n}(X)\cdot \underset{\sim}{r}(X))\, d\underset{\sim}{t}}{\int\int_S \underset{\sim}{r}(X)\cdot \underset{\sim}{n}(X) \Psi(\underset{\sim}{n}(X)\cdot \underset{\sim}{r}(X))\, d\underset{\sim}{t}} ,$$

where $\Psi(y)$ is an indicator function that is unity if y is non-negative , and 0 otherwise. (The arguments of the function $X(t)$ have been suppressed.) The purpose of the function Ψ is to ignore any surfaces that are not visible to the viewer at $r(X)$. Although the above technical description of the emissivity over a surface does not include self-shadowing of the surface, we do take shadowing into account computationally.

One feature that is immediate from the mean emissivity is that if one models the mean slope of the surface by a flat plate having a tangent vector T, then $n \cdot T = 0$ defines the normal to the surface. If the emissivity is described by i and ii above and if v is a unit viewvector, then the maximum value of $\varepsilon(\theta)$ occurs when $\theta = \arccos(n \cdot v) = 0$, which implies that n and v are collinear. It is obvious given a non-zero slope that for views looking straight down, ε is less than unity. As the the angle from the zenith is increased towards the normal, ε increases until it reaches its maximum value and then decreases to a positive minimum value when the viewing vector is near grazing. However, one must not take the grazing analysis too seriously because at that view angle, self-shadowing becomes dominant.

In order to perform our computer analysis, emissivity for the optical wavelength of 10 microns was estimated for the rough sea state by simplifying the two dimensional model to one dimension after generating the surface at a given wing speed. A view point and view direction is selected by specifying a range, azimuth, and colatitude. The range is measured in units of footprint dimension, L, from the center of the footprint; colatitude is measured from the zenith; azimuth is measured clockwise from the downwind direction. Thus our coordinate system has the following labelling : z = zenith, x_1 = downwind, x_2 = crosswind.

A one-dimensional profile of the rough surface is taken by collecting the elevation and slope values along a chosen azimuth. Since our profile is discrete, the profile consists of elements or facets. This array of facets defines a footprint of length equal to 512 times a unit facet length. View directions are confined to the vertical plane defined by the profile azimuth. A ray is then drawn from each facet to the viewpoint. If a ray strikes another portion of the surface before reaching the viewpoint, the facet from the which the ray emanated is said to be in shadow.

Emissivity computer computations are discrete spatial averages over the profile. The discrete model for the mean emissivity over a surface is given by:

$$\langle \hat{\varepsilon}(\theta(r(0))) \rangle = \Sigma \varepsilon_i A_i / \Sigma A_i \qquad 2\text{-}1$$

where each sum is taken over all visible facets in the profile, (excluding those in shadow and/or facing away from viewer). A_i is the projected area of the ith (unit) facet. ε_i is the emissivity of the ith facet, which is constant across the facet with amplitude determined by a scalar function of θ_i known for flat (smooth) water. θ_i is the angle made by the local view vector (vector pointing to the view point, from the center of the facet) and the facet's normal.

The projected area A_i is simply

2-2 $$A_i = e_{vi} \cdot e_{ni},$$

where e_{vi} is the unit view vector to the ith element, and e_{ni} is the unit normal of the ith facet. The facet emissivity is:

2-3a $$\varepsilon_i = \varepsilon(\theta_i),$$

2-3b $$\theta_i = \mathrm{acos}(\, e_{vi} \cdot e_{ni}),$$

where $\varepsilon(\theta)$ is the emissivity of smooth water.(Note that transmittance (at 10 microns) is negligible, and we assume the surface is in thermal equilibrium .) Also,

2-4a $$\varepsilon(\theta) = 1.0 - \rho(\theta)$$

2-4b $$\rho = 1/2 * (\, \rho_1 + \rho_2 \,)$$

where the perpendicular and parallel components of the reflectivity are ρ_1 and ρ_2 , respectively.

An average emissivity is calculated for each position of the viewpoint as it is placed, with constant range, at different look angles. Figure 3 shows, for surfaces derived from the Cox-Munk window, the variation in mean emissivity with look angle. Five emissivity curves are shown, corresponding to a smooth (wind speed = 0) sea and the four

wind speeds mentioned above, for a range equal to the dimension of the footprint and a view direction parallel to downwind (azimuth = 0).

Look angle emissivities were calculated for two view directions: downwind & crosswind, for each of two range/footprint ratios(1.0 & 10.0),and for each of the four wind speeds and three spectral ranges. Hence it is possible to analyze the four-fold dependence of emissivity on (1) wind-speed (surface roughness), (2) surface asymmetry (downwind-crosswind),(3) sensor range, and (4) the proportionate influence of short and long wavelength wind-waves present.

In [14], it is shown that a very small relative change in emissivity can correspond to a surprisingly large change in relative temperature. For a reference temperature of 300 K, a 1.0 percent change in emissivity relates approximately to 0.5 K change in temperature. We derive an expression for the apparent temperature by assuming a fixed radiance,I, and equate two equivalent gray body emissions:

2-5a $$I = \langle\varepsilon_0\rangle \cdot I_{bb}(T_0) = \langle\varepsilon\rangle \cdot I_{bb}(T),$$

where I_{bb} is the Planck black body radiation law as a function of temperature, , and $\langle\varepsilon_0\rangle$ and T_0 are known (reference) emissivity and temperature, respectively. (Since I is fixed, T_0 constrains $\langle\varepsilon_0\rangle$.)

Equation 2-5a implies

2-5b $\langle\varepsilon\rangle/\langle\varepsilon_0\rangle = (\exp(B/T) - 1) / (\exp(B/T_0) - 1),$

and solving for T yields

2-6 $T(\langle\varepsilon\rangle) = B / \mathrm{Log}\{ 1 + \langle e\rangle/\langle e0\rangle \cdot (\exp(B/T_0)-1)\},$

where B is a constant. Figure 5 shows the temperature curves derived from the emissivity curves of Fig. 3 by using expression 2-6 and a reference temperature of 300 K. Since small deviations in emissivity are magnified through the temperature inference we have chosen to compare the temperature, rather than emissivity in Figs. 6 through 10. This effect can be seen by considering the temperature difference between two emissivities that close together. In particular, let δ be small .. Then

$$T(\varepsilon + \delta) - T(\varepsilon) = -BC\delta/[(1+\varepsilon C)\ (\log(1+\varepsilon C))^2\ ] + O[\delta^2\ ],$$

where C is a constant depending on T_0. Since ε is small at near grazing, then by expanding the log function , the temperature difference is of the order δ/ε^2. Therefore, for angles corresponding to a near grazing viewpoint, the equivalent temperature is seen to be magnified.

3. General Discussion : The four-fold dependance of emissivity, and hence temperature, derives from the the geometrical nature of the optics. We describe our surface as a large collection of small flat facets. Each facet is defined by its spatial position and the orientation of its unit normal . The optical properties of the collection of facets, namely emission and reflectance, are prescribed by equations 2-1 through 2-4 above.

The emissivity of the surface, which is an averaged quantity, will be affected by the total slope variance as well as the elevation variance. For a fixed look angle, a flat horizontal surface will have a different average emissivity than a rough surface. The non-zero slope variance of the rough surface guarantees that some percentage of surface facets will have normals which deviate substantially from the vertical. These facets will contribute to an overall change in average emissivity. The non-zero elevation variance will contribute to the change in emissivity by inducing surface self-shadowing, which clearly does not occur in a flat surface.

Elevation and slope variance provide measures of the surface roughness. From Fig. 1 we note that slope variance depends not only on wind speed, but also on the spectral composition of the surface. Each spectral window sets the range of small, medium, and large wavelengths used in the surface composition. The capillary window defines a preference for small wavelengths, while the sub-Leyken/Rosenberg emphasizes large wavelengths. From Fig. 1

we see small wavelengths contribute more to the total slope variance, for all wind speeds, than large wavelengths.

Given a spectral window, the power spectral density is used to specify the relative proportion of the contribution from each wavelength to the surface. In as much as the spectrum has an angular dependence, we can expect the elevation and slope variance to also have some angular dependance. Wind velocity, spectral composition, and the angular variation of the spectrum all contribute to the elevation and slope variance of the surface. Three of the four quantities which we use to describe measured temperature are directly related to the geometric properties of the surface, the fourth is related to the geometry of the measurement.

Relative fluctuations of facet normals about the vertical imply fluctuations about the viewing vector. Equations 2-3 show that the important optical quantities are the angles between the facet normals and the rays drawn to the viewpoint; i.e. the view vectors. While the slope variance of the surface affects these angles, so does the position of the of the view point. If the view point is placed at an infinite range, the view vectors would be constant across the surface. If, however, the viewpoint is placed at a finite range, each ray or local view vector will be unique. The distribution of angles (between facet normals and local view vectors) will be a function of the view point position and the scale of the footprint. We can combine the view point position and footprint size into one parameter:

r/f, the ratio of range to foot- print length, a dimensionless quantity.

The behavior of inferred temperature with respect to each of the four 'parameters' discussed above is shown for some typical cases in plots 6 through 10.

4. Discussion of Plots : Figure 1 shows three curves and a set of measurements with error bars. The measurements are derived from the Cox-Munk expression for total slope variance as a function of wind speed. Each curve represents integration of the slope spectral density over each of the three spectral windows. The solid curve, which approximates the measurements, represents the integration over the Cox-Munk spectral region (k_{max} = 1.20), while the dashed curve represents the integration of the slope spectrum over the sub-Leyken/ Rosenberg region (k_{max} = 0.359). The dotted curve represents integration over the capillary region (k_{max} = 5.0).

For all wind speeds in the range of 3.0 to 15.0 m/s, the total slope variance of the sub-Leyken/Rosenberg range of wind-waves is substantially lower than the Cox-Munk values. The integration for k_{max} = 5.0 represents an approximation to the capillary spectral range (see Table 1 for the precise values of kmax and corresponding wavelengths). For all wind speeds shown, the total slope variance of the capillary spectral range is substantially greater than the Cox-Munk values

Figure 2 shows a simple grid plot of a sea surface constructed form our model. The surface corresponds to a wind speed of 9.97 m/s using the Cox-Munk window. The smallest wavelength present in the surface is equal to $2\pi/kmax$, and the largest wavelength is equal to $2\pi/(kmax/(N/2)) = (N/2) * (\text{smallest wavelength})$. We define the unit facet length to equal 1/2 * (smallest wavelength); the model gives a grid of 512 x 512 facets. For the Cox-Munk window the unit facet area is approximately 2.6 x 2.6 cm**2.

Figure 3 shows a typical set of emissivity results. The emissivity curves give the average emissivity evaluated at each look angle. Graphed are emissivity curves for a flat surface and for rough surfaces due to the four stated wind speeds. The view point and view direction are defined by the r/f ratio of 1.0 and an azimuth of 0.0 (downwind). The behavior of the emissivity curves is similar to results in [10] , although the optical wavelength Sidran used is 1.0 micron while we use 10.0 microns. Like the Sidran results, the curves show a drop in emissivity that is more rapid at small look angles, but less rapid at large angles (near grazing), than the behavior of a flat sea. At a look angle between 62 & 64 degrees the rough surface emissivity curves intersect the flat surface curve. At this critical range of angles, the emissivities of all wind roughened surfaces (including zero velocity) are approximately identical to each other .

Figure 5 shows the temperature curves inferred from the emissivity curves of Fig. 3. For look angles less than 62 degrees all roughened surfaces are cooler than the flat surface. For look angles greater than 64 degrees all roughened surfaces are hotter than the flat sea. In the critical range of 62-64 degrees, all measured temperatures are approximately equal.

Figures 6 and 7 show temperature difference curves to emphasize the behavior with respect to view direction and range. In each set of curves, the temperature differences are negligible for look angles below 30 degrees. For look angles greater than 30 degrees, the crosswind temperatures are greater than the downwind, and the short range temperatures are greater than the long range.

Figures 8, 9, 10 depict temperature difference curves which compare the results of the three spectral windows. In Fig. 8 temperatures derived from a sub-Leyken/Rosenberg surface are subtracted from the Cox-Munk temperatures, showing that a surface comprised of short wavelength water waves will appear hotter. Figures 9 & 10 show essentially the same results.

5. Conclusions :

Peltzer[8] reports a thermal wake distinct from the surrounding ocean surface which cannot be accounted for by upwelling of cooler water from below the surface. If one assumes the ship's passage through water acts to dampen the

short wavelength portion of the existing wind waves [1b] , the cooler measured temperatures are partly explained by our results. The wake has an entirely different surface characteristic than the surrounding water [1b] , and hence an associated change in emissivity. In [8], it is also reported that an apparent dependance of temperature measurements of the wake on sensor altitude exist. This could be a direct result of the range dependence we discussed.

Temperatures are generally inferred from radiance measurements by assuming a constant emissivity across the surface. Liu and Katsaros [6] use a constant emissivity of 0.86 in their evaluation of the spatial variation of sea surface temperature across a 70 kilometer region. Our temperature curves of Fig. 5 show an emissivity of 0.86 for a flat sea at a look angle of 75 degrees. In this area our curves show variations of temperature greater than 2 degrees Kelvin . Liu and Katsaros measure spatial temperature variations in the range of 0.8 degrees (peak-peak) before subtraction of sky reflection, and 0.3 degrees after subtraction of sky reflection.

If one is to infer temperature from a fixed emissivity while ignoring surface geometry, the radiance should be observed at an angle in the range of 62-64 degrees. At this angle it is reasonably safe to assume a constant emissivity of 0.95 for all wind conditions. Liu-Katsaros show a plot of measured temperature as a function of distance over the horizontal range of 70 kilometers. The peak to peak variation in temperature is less than 0.3

degrees . Our results indicate that a change in emissivity along the spatial range of the measurements, which could be due to a possible change in spectral composition of the waves or a change in wind direction or speed, is likely to introduce errors in the measured temperature of a magnitude equal to or greater than peak-peak variations reported in [6].

Finally we wish to stress the significance of the wind wave spectral dependance shown in Figs. 8-10. Our analysis utilizes the simplest of wind wave surface models. Nothing has been said about surface waves generated by phenomena other than those which define the fully developed sea (steady winds acting over large fetches of infinitely deep water for sufficiently long periods of time to engender 'steady states'). We find a significant influence due to capillary waves on the overall optical properties of the surface, which should not be ignored, as Wilf & Manor [14] suggest.

REFERENCES

[1a] Chapma., R.D. and Irani, G.B., Errors in estimating slope spectra from wave images, Applied Optics, **20**, 3645, 1981.

[1b] Cooper, A.L., Interactions between ocean surface waves and currents, NRL Memorandum Report 5755, 1986.

[2] Cox, C. and Munk, W., Measurement of the roughness of the sea surface from photographs of the sun's glitter, J. Opt. Soc. Am., **44** pp. 838-850, 1954.

[3] Grachev, A.A., Convective cooling of a fluid from a free surface, Izv., Atmospheric and Oceanic Physics, **19** pp. 379-385, 1983.

[4] Hill, R.L., Laboratory Measurements of heat transfer, wind velocity profiles, and temperature structure at an air/water interface, NRL Report 7212, 1970.

[5] Hudson, R.D., Infrared System Engineering, John Wiley and Sons, New York, 1969.

[6] Katsaros, K.B. and Liu, W.T., Radiative sensing of sea surface temperature, in Instruments and Methods in Air-Sea Interaction, ed. Dobson, F., Hasse, L., Davis, R., pp. 293-317, Plenum, New York, 1980.

[7] McLeish, W., Spatial spectra of ocean surface temperatures, J. Geo. Phys. Res., **75**, pp. 6872-6877, 1970.

[8] Peltzer, R.D., Remote sensing of the USNS Hayes wake, NRL Memorandum Report 5430, 1984.

[9] Pierson, W.J. and Stacy, R.A., The elevation, slope, and curvature spectra of a wind roughened sea surface, NASA Contractor Report, CR-2247, 1973.

[10] Sidran, M., Broadband reflectance and emissivity of specular and rough water surfaces, Applied Optics, B20, pp. 3176-3183, 1981.

[11] Singh, S.M. and Warren, D.E., Sea surface temperatures from infrared measurements, in Remote Sensing Applications in Marine Science and Technology, ed. A.P. Cracknell,pp. 231-262, D. Reidel Publishing Company, New York, 1983.

[12] Spangenberg, W.G. and Rowland, W.R., Convective circulation in water induced by evaporative cooling, Physics of Fluids, **4**, 743-750, 1961.

[13] Street, R.L., Wang, C.S., McIntosh, D.A., Miller, A.W. and Fluxes through the boundary layers at an air-water interface, in Turbulent Fluxes Through the Sea Surface, Wave Dynamics, and Prediction, eds. A. Favre and K. Hasselmann, pp. 99-120 Plenum Press, New York, 1978.

[14] Wilf, I. and Manor Y., Simulation of sea surface images in the infrared, Applied Optics, **23**, pp. 3174-3180, 1984.

TABLE 1

SPECTRALWINDOW	KMAX(RAD/CM)	WIND SPEED (M/S)
CoxMunk	1.20	all wind speeds
SubLeyken/Rosenberg	0.359	all wind speeds
Capillary	4.3845	3.46
Capillary	4.8469	5.61
Capillary	5.2209	7.63
Capillary	5.6369	9.97

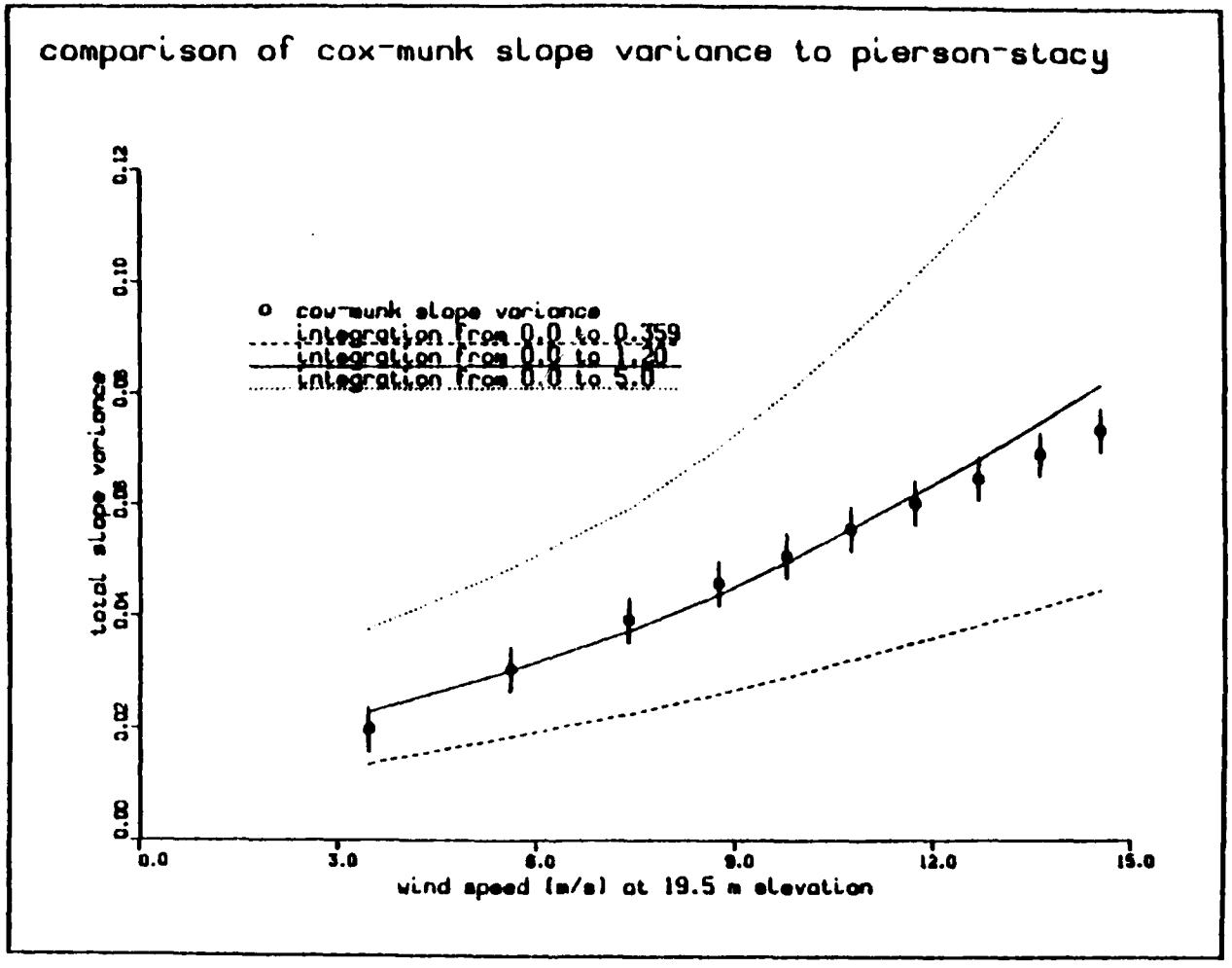

Fig. 1 — Comparison of Cox-Munk slope variance to Pierson-Stacy

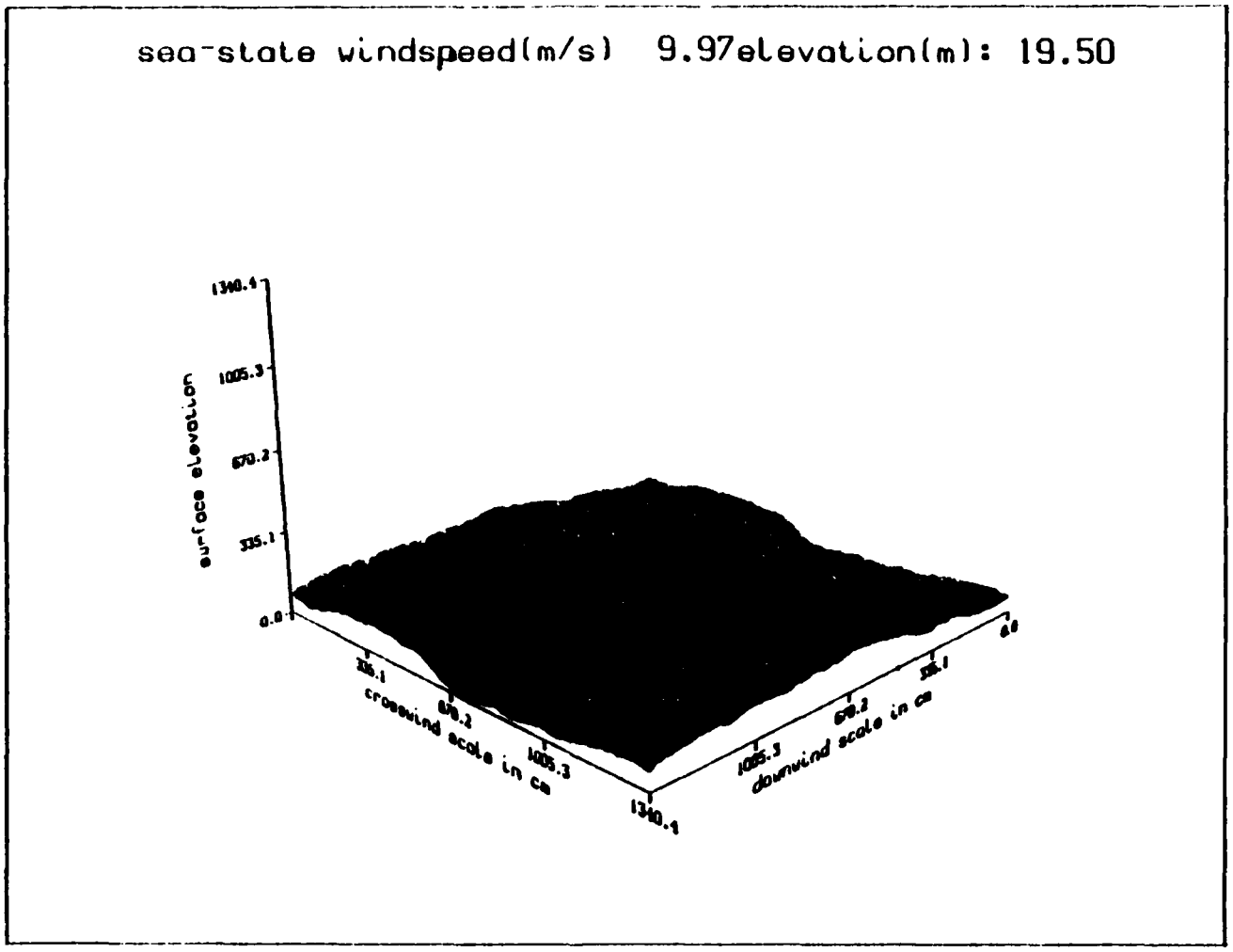

Fig. 2 — Example of a synthetic rough sea state

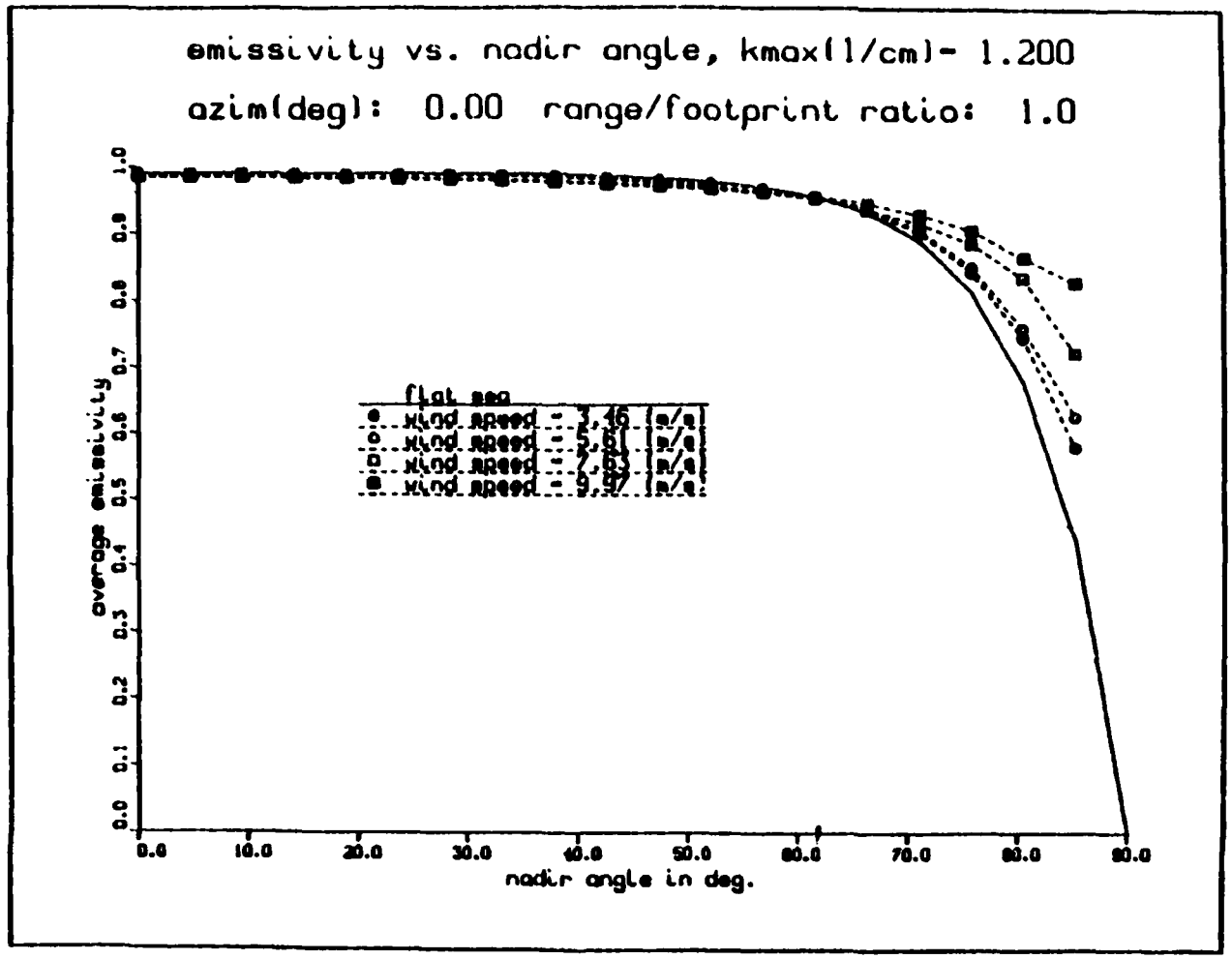

Fig. 3 — Emissivity vs Angle

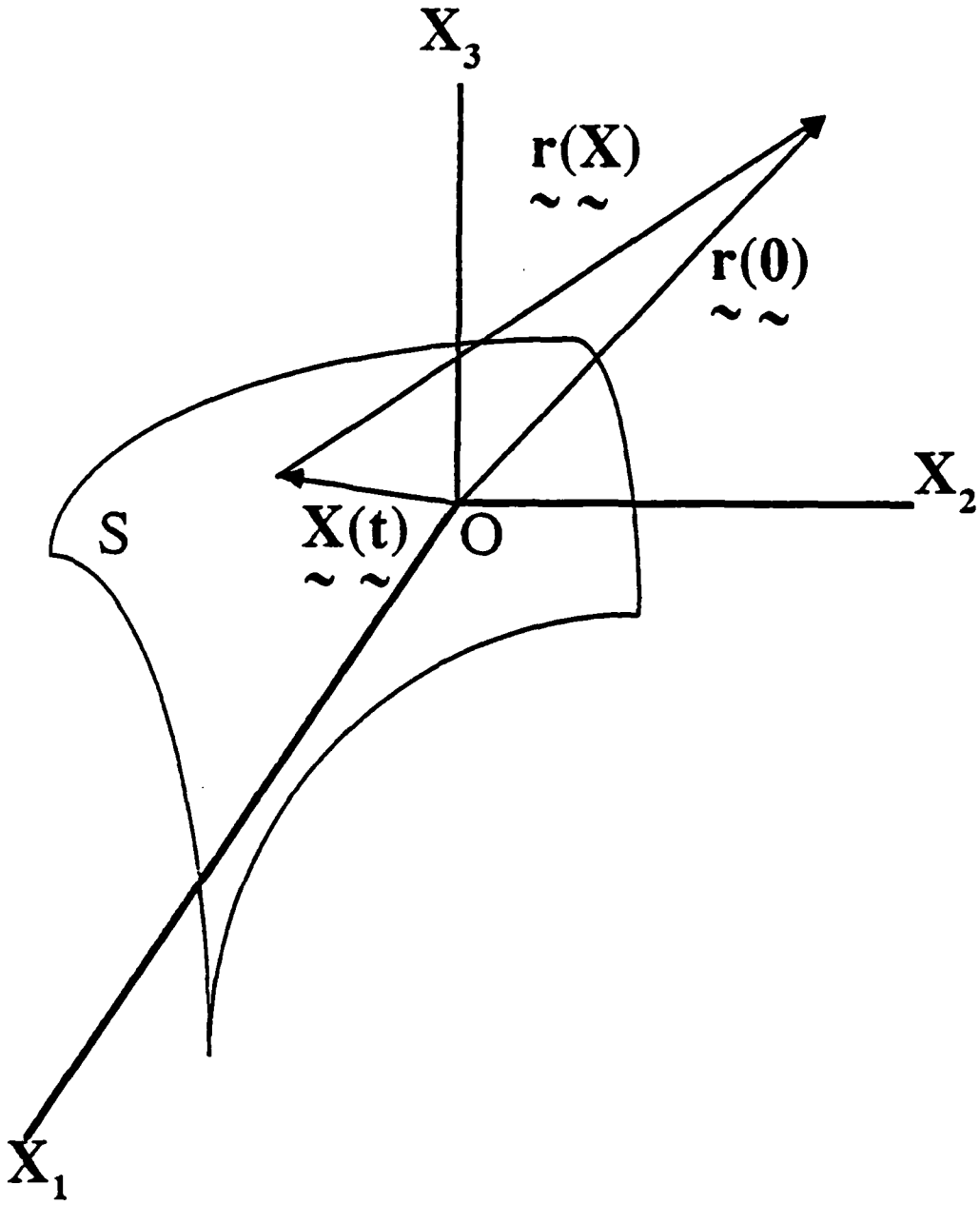

Fig. 4 — Geometry of the view of a general surface S

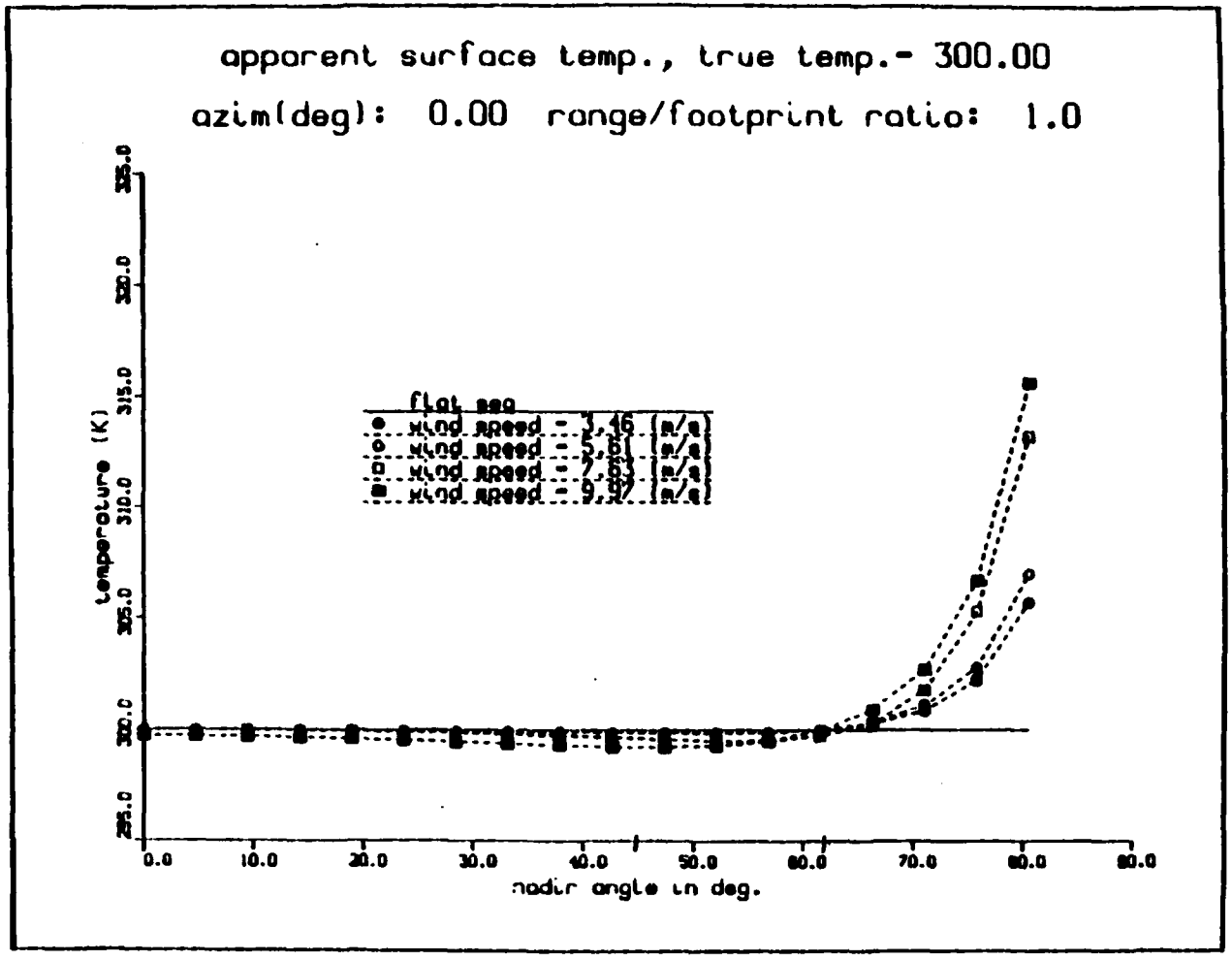

Fig. 5 — Apparent temperature vs angle

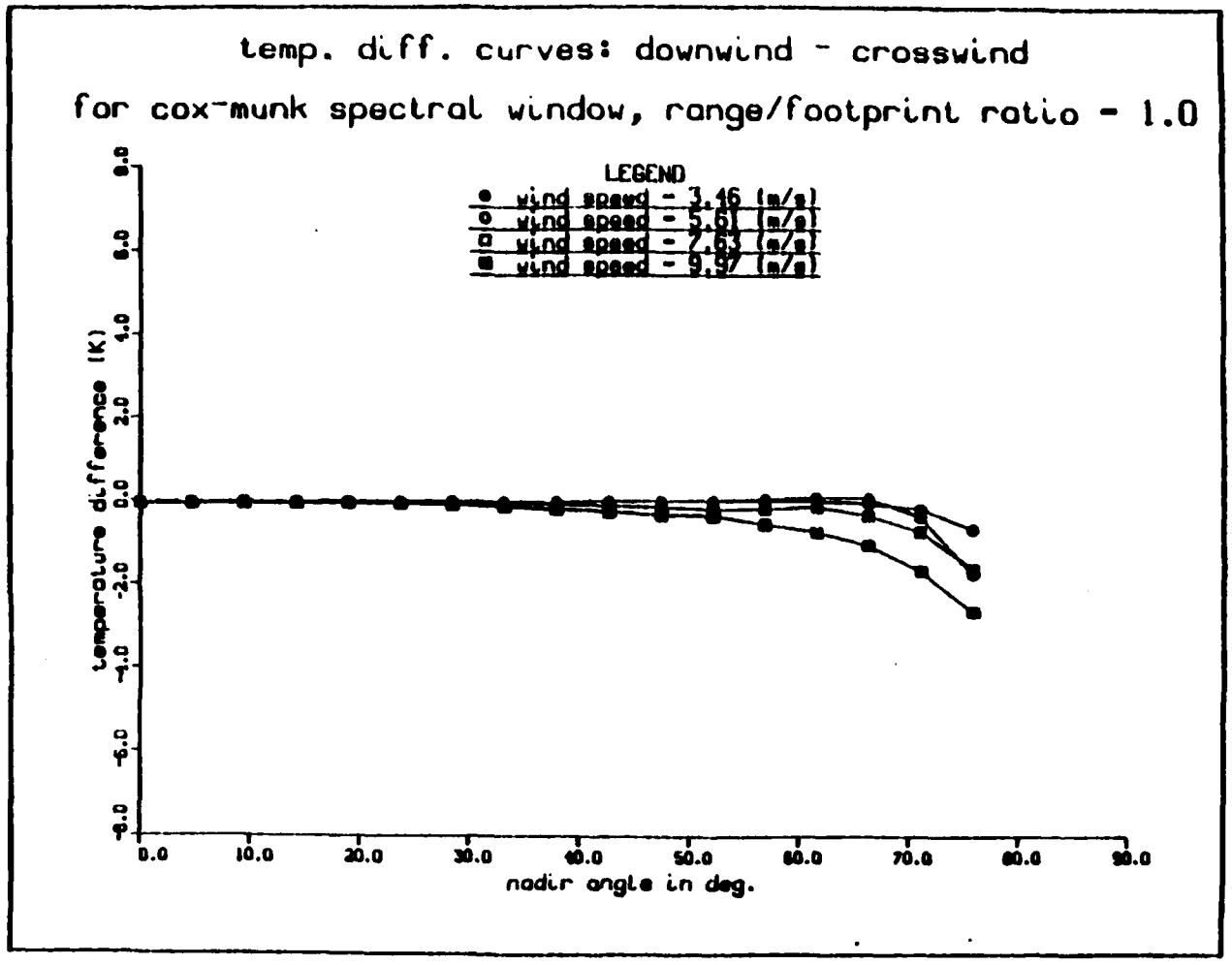

Fig. 6 — Downwind-crosswind temperature difference vs angle

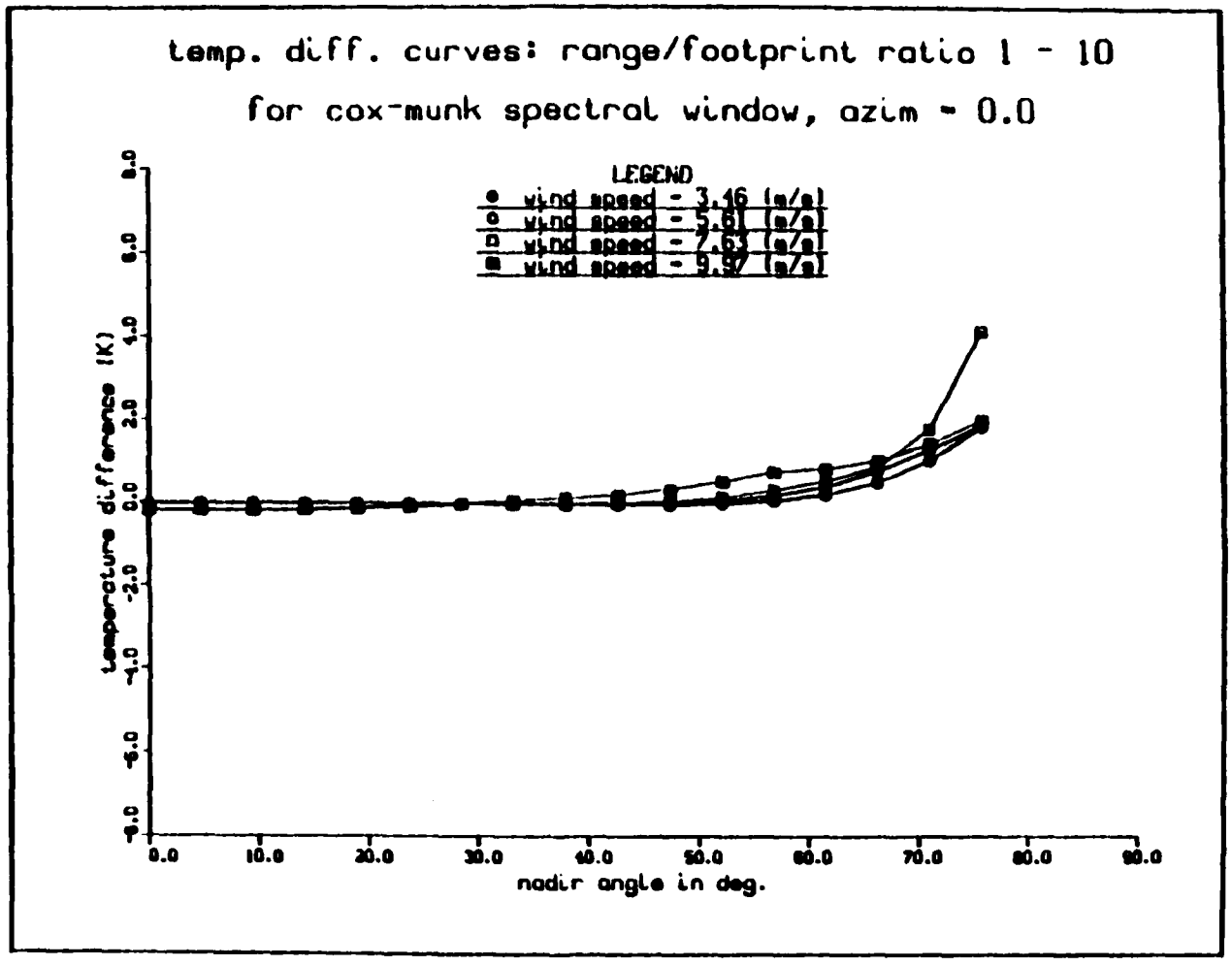

Fig. 7 — Range-footprint temperature difference vs angle

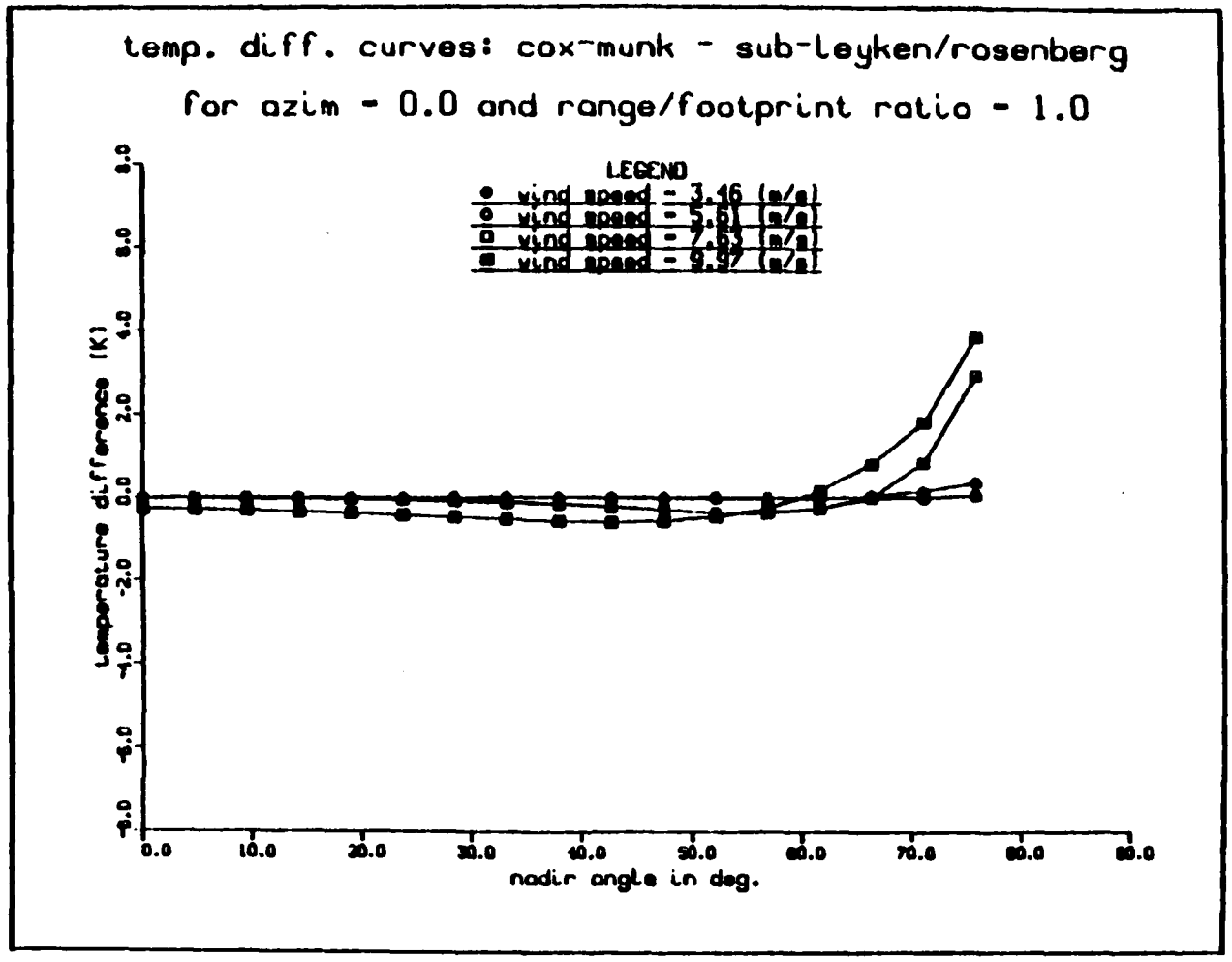

Fig. 8 — Cox Munk—sub-Leyken/Rosenberg temperature difference vs angle

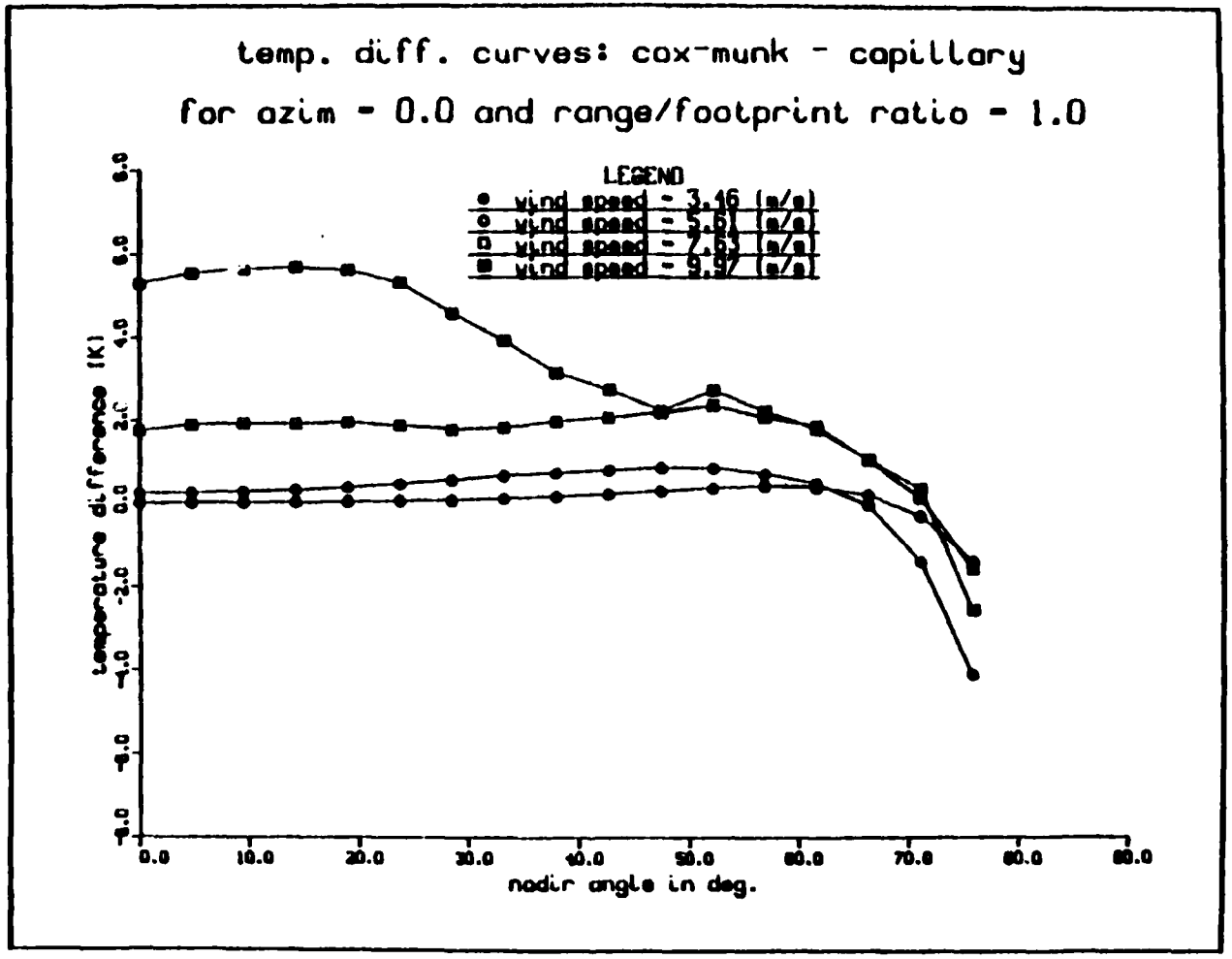

Fig. 9 — Cox-Munk—Capillary temperature difference vs angle

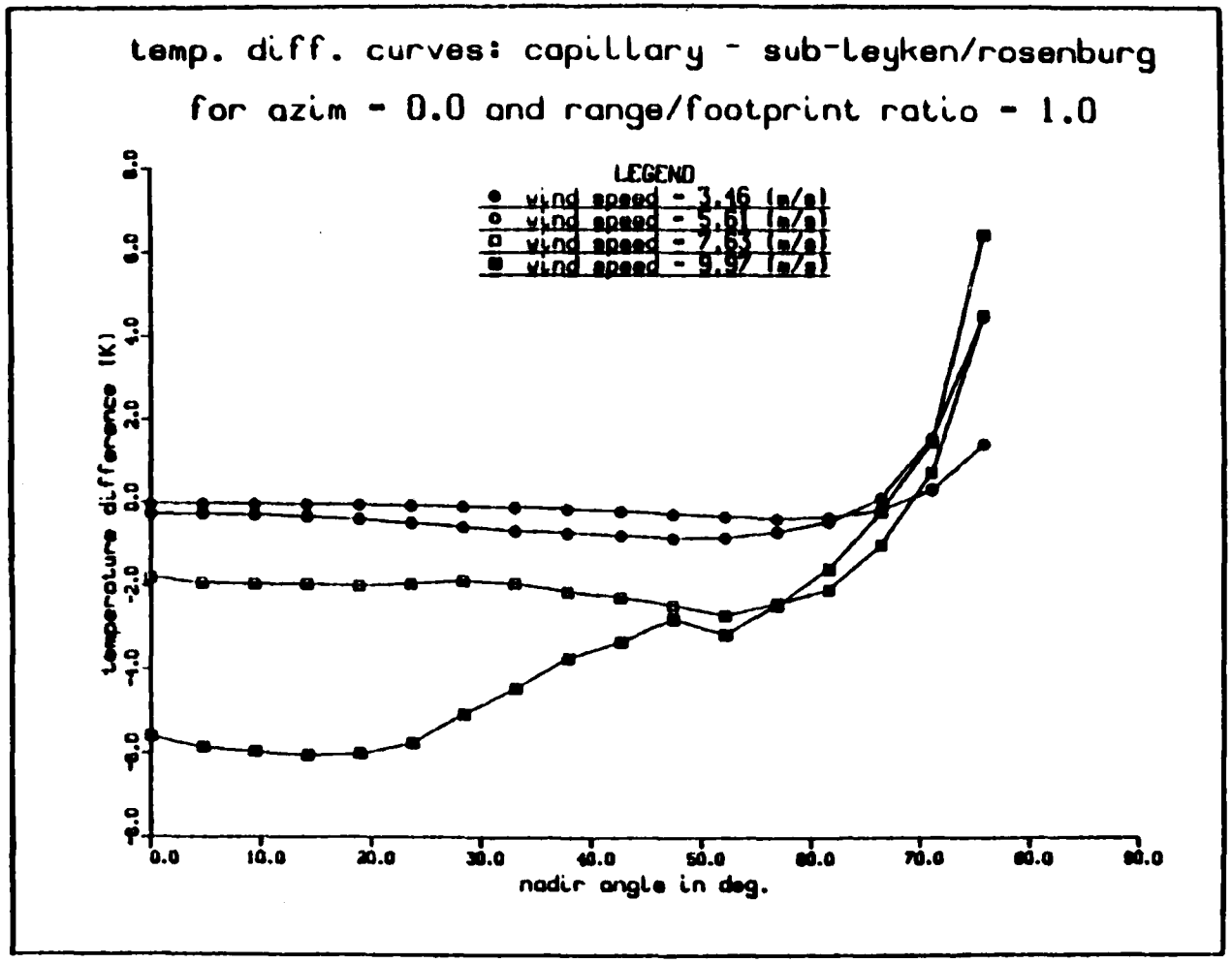

Fig. 10 — Capillary—sub-Leyken/Rosenberg temperature difference vs angle

END

10-86

DTIC